ARTICLES
PUBLISHED ONLINE: 17 APRIL 2011 | DOI: 10.1038/NMAT3011
nature materials

Low-temperature fabrication of high-performance metal oxide thin-film electronics via combustion processing

Myung-Gil Kim[1], Mercouri G. Kanatzidis[1]*, Antonio Facchetti[1,2]* and Tobin J. Marks[1]*

The development of large-area, low-cost electronics for flat-panel displays, sensor arrays, and flexible circuitry depends heavily on high-throughput fabrication processes and a choice of materials with appropriate performance characteristics. For different applications, high charge carrier mobility, high electrical conductivity, large dielectric constants, mechanical flexibility or optical transparency may be required. Although thin films of metal oxides could potentially meet all of these needs, at present they are deposited using slow and equipment-intensive techniques such as sputtering. Recently, solution processing schemes with high throughput have been developed, but these require high annealing temperatures (T_{anneal} > 400 °C), which are incompatible with flexible polymeric substrates. Here we report combustion processing as a new general route to solution growth of diverse electronic metal oxide films (In_2O_3, a-Zn-Sn-O, a-In-Zn-O, ITO) at temperatures as low as 200 °C. We show that this method can be implemented to fabricate high-performance, optically transparent transistors on flexible plastic substrates.

Large-area, flexible macroelectronics promises lower fabrication costs and new functionality in applications as diverse as transparent flexible displays, conformal sensor arrays, radio-frequency identification (RFID) tags, flexible solar cells, and integration of logic circuits on flexible substrates by high-throughput roll-to-roll processes[1–6]. In addition to maximizing circuit performance, scaling up of substrate size and cost-effective fabrication are key issues in this emerging field[1–3]. Note that conventional electronics using single crystal silicon wafers are capital-intensive and of limited potential for large-area devices, especially when optical transparency and mechanical flexibility are desired. Although these limitations are partially addressed with amorphous silicon (a-Si:H), it is limited in performance (mobility, current-carrying capacity, transparency) for these emerging applications. Therefore, new materials and fabrication approaches based on scientific understanding will be required for all the material components of thin-film transistors (TFTs), including the semiconductor, gate dielectric and conductors.

Regarding candidate semiconductors, organics and some nanomaterials are solution-processable to yield TFT performance comparable to a-Si:H (field-effect mobility $\mu \sim 1\,cm^2\,V^{-1}\,s^{-1}$; refs 7–12) whereas the more expensive laser crystallization of a-Si:H or mechanical transfer of semiconducting objects affords larger areas and $\mu \sim 100\,cm^2\,V^{-1}\,s^{-1}$, with each approach having both strengths and limitations[13–15]. For gate insulators, solution-processable high-κ self-assembled nanodielectrics, ion-gels, and polarizable ionic materials[5,16–18] can compensate for the low semiconductor mobilities, high operating voltages, and trapped interfacial charge in TFTs fabricated with the aforementioned solution-processed semiconductors. Finally, for electrodes, solution-deposition routes for conducting oxides, noble metals, and carbon materials could in principle replace lithographic and vacuum deposition techniques, but these currently require high annealing temperatures and/or expensive materials[4,19–21]. Therefore, to address current macroelectronics challenges, further materials and processing advances are essential.

Recently, oxide semiconductor films grown by physical vapour deposition (PVD) techniques have demonstrated electrical performance comparable to poly-Si and with excellent environmental stability and optical transparency, arising from wide bandgaps[22–24]. Several laboratories have also reported solution-processed oxide TFTs with device metrics comparable to PVD-derived devices[25–30]. However, the condensation, densification, and impurity removal steps of solution oxide film processing typically require annealing above 400 °C, which is incompatible with most flexible plastic substrates and risks complications, such as cracking induced by thermal expansion coefficient mismatch[3,31]. In limited cases, for example, nanocrystalline ZnO suspensions, processing temperatures can be lowered to 150–250 °C using special precursors or doping techniques, however the mobilities achieved are no greater than $\sim 1\,cm^2\,V^{-1}\,s^{-1}$ (refs 32–36). At present there exist no effective general approaches to achieving low-temperature solution-processed oxide TFTs with a performance exceeding that of a-Si:H.

Here, we report a new and general strategy for fabricating solution-processed metal oxide TFTs at much lower annealing temperatures, T_{anneal} as low as 200 °C, for all TFT electrical components, using self-energy generating combustion chemistry. These low temperatures enable fabrication of high-performance devices on typical flexible substrates such as a transparent AryLite polyester. Moreover, we show that tuning the gate dielectric–semiconductor interface greatly enhances performance, yielding In_2O_3 semiconductor/amorphous alumina gate dielectric TFTs with electron mobilities of $40\,cm^2\,V^{-1}\,s^{-1}$ and $13\,cm^2\,V^{-1}\,s^{-1}$ at $T_{anneal} = 250$ °C and 200 °C, respectively. Finally, this approach is implemented for flexible TFTs to achieve an electron mobility of $6\,cm^2\,V^{-1}\,s^{-1}$ for $T_{anneal} = 200$ °C on transparent polymer substrates.

[1]Department of Chemistry and the Materials Research Center, Northwestern University 2145 Sheridan Road, Evanston, Illinois 60208, USA, [2]Polyera Corporation, 8045 Lamon Avenue, Skokie, Illinois 60077, USA. *e-mail: m-kanatzidis@northwestern.edu; a-facchetti@northwestern.edu; t-marks@northwestern.edu.

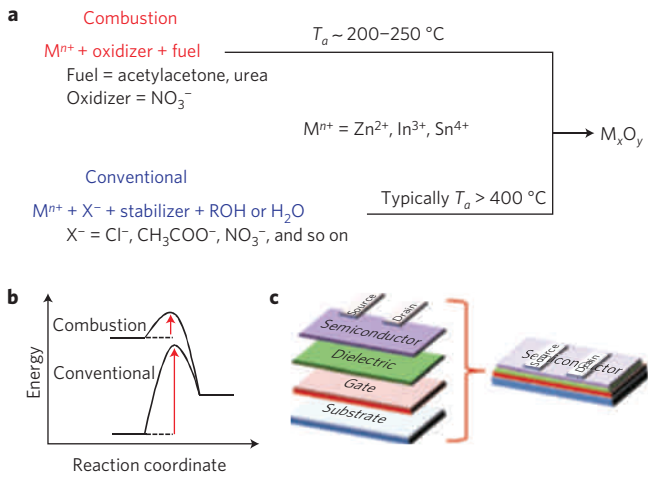

Figure 1 | Low-temperature solution-processing principles for metal oxides and fabricated device structures. a, Depiction of the two different synthetic approaches. **b**, Energetics of combustion synthesis-based processes versus conventional processes. **c**, Top-contact bottom-gate TFT device structure used in this study.

For low-temperature solution-based oxide film fabrication, a promising approach would be via a localized heating mechanism analogous to low-temperature poly-Si laser crystallization[13,14]. However, for the present wide bandgap oxides, this would require expensive ultraviolet lasers and would risk damaging other materials in the device[37]. Combustion processing can achieve the energy-efficient synthesis of bulk materials such as chalcogenides, III–V semiconductors, carbides, binary oxides, and intermetallics[38–40]. The self-generated heat of synthesis provides a localized energy supply, eliminating the need for high, externally applied processing temperatures. In the present study, a redox-based combustion synthetic approach is applied to oxide thin films, using acetylacetone or urea as a 'fuel' and metal nitrates as oxidizers[41]. As an example, the balanced and highly exothermic oxidizer + fuel pair for the combustion synthesis of ZnO is shown in equation (1)

$$3Zn(NO_3)_2 \cdot 6H_2O_{(s)} + 5 \left(O=C(H_2N)(NH_{2\,(s)}) \right) \longrightarrow$$

$$3ZnO_{(s)} + 8N_{2(g)} + 28H_2O_{(g)} + 5CO_{2(g)}$$

$$\Delta H_{298\,K} = -2320.4\,\text{kJ and } T_{ad} \sim 700\,^{\circ}\text{C} \qquad (1)$$

where $T_{ad} \sim 700\,^{\circ}\text{C}$ can be achieved under ideal adiabatic conditions. It can be seen that combustion synthesis offers many attractions for film solution processing. First, the generation of high local temperatures without a furnace enables low-cost large-scale bulk syntheses, and the high self-generated energies can convert precursors into the corresponding oxides at low process temperatures. In contrast, oxide formation via conventional precursors based on metal hydroxide and/or alkoxide conversion is endothermic, requiring significant external energy input to form metal–O–metal lattices, whereas combustion synthesis is exothermic, not requiring external energy input once ignited. These differences are illustrated in Fig. 1a,b. Furthermore, conventional processes and precursors typically require high temperatures for oxidizing organic impurities to achieve phase-pure products, whereas in combustion reactions with balanced redox chemistry, the atomically local oxidizer supply can efficiently remove organic impurities without coke formation.

In Fig. 2a and Supplementary Fig. S1, thermogravimetric analysis (TGA) and differential thermal analysis (DTA) data are plotted for various precursors of In_2O_3, a-IZO ($In_{0.7}Zn_{0.3}O_{1.35}$ for combustion, $In_{1.0}Zn_{1.0}O_{2.5}$ for conventional precursors), a-ZTO ($Zn_{0.3}Sn_{0.7}O_{1.7}$ for combustion, $Zn_{1.0}Sn_{1.0}O_{3.0}$ for conventional precursors), and $In_{0.9}Sn_{0.1}O_{1.55}$ (ITO)—important materials in oxide electronics. The stoichiometries of the a-IZO and a-ZTO films reported here are those found to afford optimum TFT performance, and are compared with compositions from literature optimized for high-temperature processing. These compositions can also be prepared by combustion processing, as judged from the thermal analysis and TFT data shown in Supplementary Fig. S1c,d, but do not afford as high TFT performance. All of the combustion precursor systems exhibit substantially lower complete conversion temperatures ($T_{completion}$ < 200–300 °C) than the conventional oxide systems ($T_{completion}$ > 500–600 °C; refs 19, 26–28,30). Unlike conventional systems, which exhibit broad endotherms for oxide lattice formation and exotherms for organic impurity removal, the combustion systems, with the exception of ZTO, exhibit a single, intense exotherm in the DTA that corresponds exactly to the abrupt mass loss in the TGA and is sufficient to drive the reaction rapidly to completion. Presented in Fig. 2, along with these conversion temperatures, are the resulting semiconductor TFT carrier mobility, μ, or contact material conductivity, σ. For the conventional precursor route, adequate device performance is typically only possible for annealing temperatures greater than that for metal oxide lattice formation or organic impurity oxidation[42,43]. However, note that, in combustion systems, the required temperature has a different meaning. That is, because the principal driving force for oxide lattice formation in combustion synthesis derives mainly from internal chemical energy, the required temperature can be described as that for reaction initiation rather than a temperature that must be continuously maintained to drive the reaction[38,40]. Interestingly, the ZTO DTA scan reveals a sharp, intense exotherm at 110 °C and a small broad endotherm around 250 °C, with corresponding abrupt and gradual mass losses (Fig. 2a). Grazing incidence angle X-ray diffraction (GIAXRD) analysis (Supplementary Fig. S2c) reveals that the film is amorphous up to 400 °C. However, these ZTO films undergo conversion to a metal oxide semiconductor around 225 °C, judging from the TFT response (see below). The initial combustion of the organic fuel with the metal nitrates at 110 °C may not be sufficient to drive the reaction to completion, so two conversion steps are observed by TGA at a moderate heating rate of 10 °C min^{-1}. Such 'chemical oven' behaviour is well established for bulk silicide and carbide combustion syntheses[40], and, in the present case, the low-temperature ignitable urea-ammonium nitrate pair exotherm is coupled to a weakly endothermic Zn–Sn–O reaction at higher temperatures and drives the reaction to completion if the ignition generates sufficient heat. Thus, on exposing the film directly to moderate temperatures (>225 °C), the internal chemical energy combined with external thermal energy induces complete reaction at significantly lower temperatures than conventional oxide systems.

In addition to thermal analysis, GIAXRD data (Fig. 3a,b; Supplementary Fig. S2a) clearly indicate combustion precursor conversion to the desired crystalline oxides, In_2O_3 and ITO, at far lower temperatures than for conventional precursors. In both combustion syntheses, phase-pure bixbyite In_2O_3 phases are formed after precursor ignition at ~200 °C. Moreover, X-ray photoelectron spectroscopy (XPS) analysis verifies complete precursor conversion to oxide. The O 1s scans in Fig. 3c,d reveal the evolution of both In_2O_3 precursor films through the annealing process, with the characteristic metal–oxygen–metal (M–O–M) lattice feature at 530.1 eV increasing with increasing T_{anneal}. Note that these results agree well with the above GIAXRD and thermal analysis data[44]. The feature at 531.6 eV is attributed to either surface or bulk In–OH species[44]. The dominant In–OH feature at low

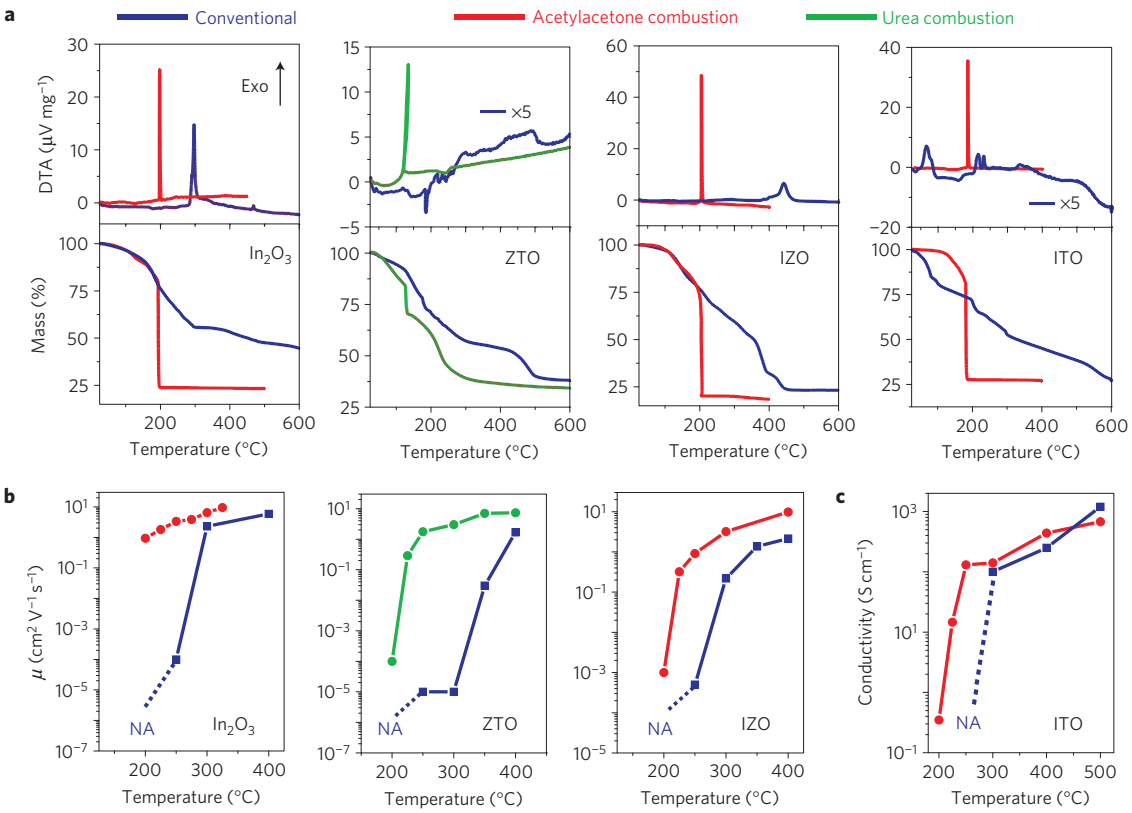

Figure 2 | Thermal analysis of the present combustion precursors versus conventional precursors and the corresponding TFT performance. Acetylacetone- and urea-based combustion precursors are denoted by red and green lines, respectively. The conventional precursor is denoted by blue lines. The blue dotted lines and NA symbols in **b** and **c** represent the extrapolated lines and data points, respectively, for inactive devices at the indicated temperatures. **a**, DTA and TGA of In_2O_3 precursors (conventional precursor from ref. 8), ZTO precursors ($Zn_{0.3}Sn_{0.7}O_{1.7}$ for combustion precursor and $ZnSnO_3$ for conventional precursor from ref. 30), IZO precursors ($In_{0.7}Zn_{0.3}O_{1.35}$ for combustion precursor and $InZnO_{2.5}$ for conventional precursor from ref. 26), and $In_{0.9}Sn_{0.1}O_{1.55}$ (conventional precursor from ref. 12). **b**, μ^{sat} versus T_{anneal} for In_2O_3 precursors, ZTO precursors, and IZO precursors. **c**, Conductivity versus T_{anneal} for ITO precursors.

annealing temperatures also confirms incomplete formation of the oxide lattice. The additional peak at 532.3 eV is assigned to adsorbed oxygen species (for example, H_2O, CO_2; ref. 44). In addition to low conversion temperatures, low carbon contamination is evident from time-of-flight secondary ion mass spectrometry (TOF-SIMS; Fig. 3e). The small XPS carbon ionization in Supplementary Fig. S3a for the 200 °C annealed combustion precursor In_2O_3 film is assigned to adventitious carbon. Thus, the SIMS data indicate trace C contamination after surface sputtering, with the In^+/CH_3^+ intensity ratio varying from ~150 at the surface to ~10,000 inside the film, corresponding to the noise level.

That the present procedure yields smooth, dense, contiguous films is confirmed by atomic force microscopy (AFM) and scanning electron microscopy (SEM), as shown in Supplementary Fig. S4a–e. Thus, films on the order of 30 nm thickness or less have very smooth surfaces (RMS roughness = 0.5–1.0 nm) with continuous coverage and negligible porosity. However, films of thickness on the order of 70 nm exhibit voids and evidence of porosity. The short diffusion length for the removal of gaseous products, such as H_2O, CO_2, and N_2, in thin films enables fast mass transport, thereby avoiding porous structures as observed in bulk combustion processing[38–40]. Furthermore, the formation of thicker, denser films is aided by multiple depositions of thin films. It should also be noted that the large surface-to-volume ratio of the films doubtless plays a role in rapid heat dissipation and suppresses crystallization of $In_{0.7}Zn_{0.3}O_{1.55}$ and $Zn_{0.3}Sn_{0.7}O_{1.7}$, which would normally crystallize above and near 600 °C, respectively[45,46].

The electronic properties of the present spin-coated/combustion-derived semiconducting In_2O_3, IZO, ZTO films were first evaluated in TFTs on p+ Si/300 nm SiO_2 substrates with thermally evaporated 30 nm Al source and drain electrodes (2,000 μm channel width, 100 μm channel length). The transistor parameters (mobility, I_{on}/I_{off}) are summarized in Table 1. The onset of TFT function in In_2O_3 matches well with the thermal analysis results. By increasing T_{anneal} to 200 °C, a mobility of ~0.81 $cm^2\,V^{-1}\,s^{-1}$, comparable to that of a-Si:H, is achieved. A continuous mobility increase is observed with increasing temperature, and is doubtless related to oxygen vacancy generation pre-filling trap sites and/or distortional relaxation reducing trap sites[32,45,46]. That the IZO onset temperature exceeds the conversion temperature can be understood by considering the following observations. From the thermal analysis data in Fig. 2a and mobility trends in Fig. 2b, IZO conversion occurs very near 200 °C, however the TFT mobility increases further with temperature, well beyond 225 °C. Furthermore, for a given processing temperature, the observed mobility is significantly lower than that of In_2O_3 films (Fig. 2b). These trends are related to insufficient oxygen vacancy generation at low processing temperatures due to strong oxygen binding by Zn^{2+}. The urea-based ZTO systems evidence slightly different trends in the thermal analysis data. Thus, even below complete conversion at ~250 °C, the TFTs exhibit a mobility of ~0.4 $cm^2\,V^{-1}\,s^{-1}$ near 225 °C. As discussed above, this can be understood in terms of the chemical oven effect, which lowers the precursor conversion temperature while simultaneously providing internal heat.

The efficacy of the present low-temperature combustion synthetic approach to electronically functional oxide films motivated an investigation of the industry standard transparent conducting oxide, Sn-doped In_2O_3 (ITO; In:Sn = 9:1). As for

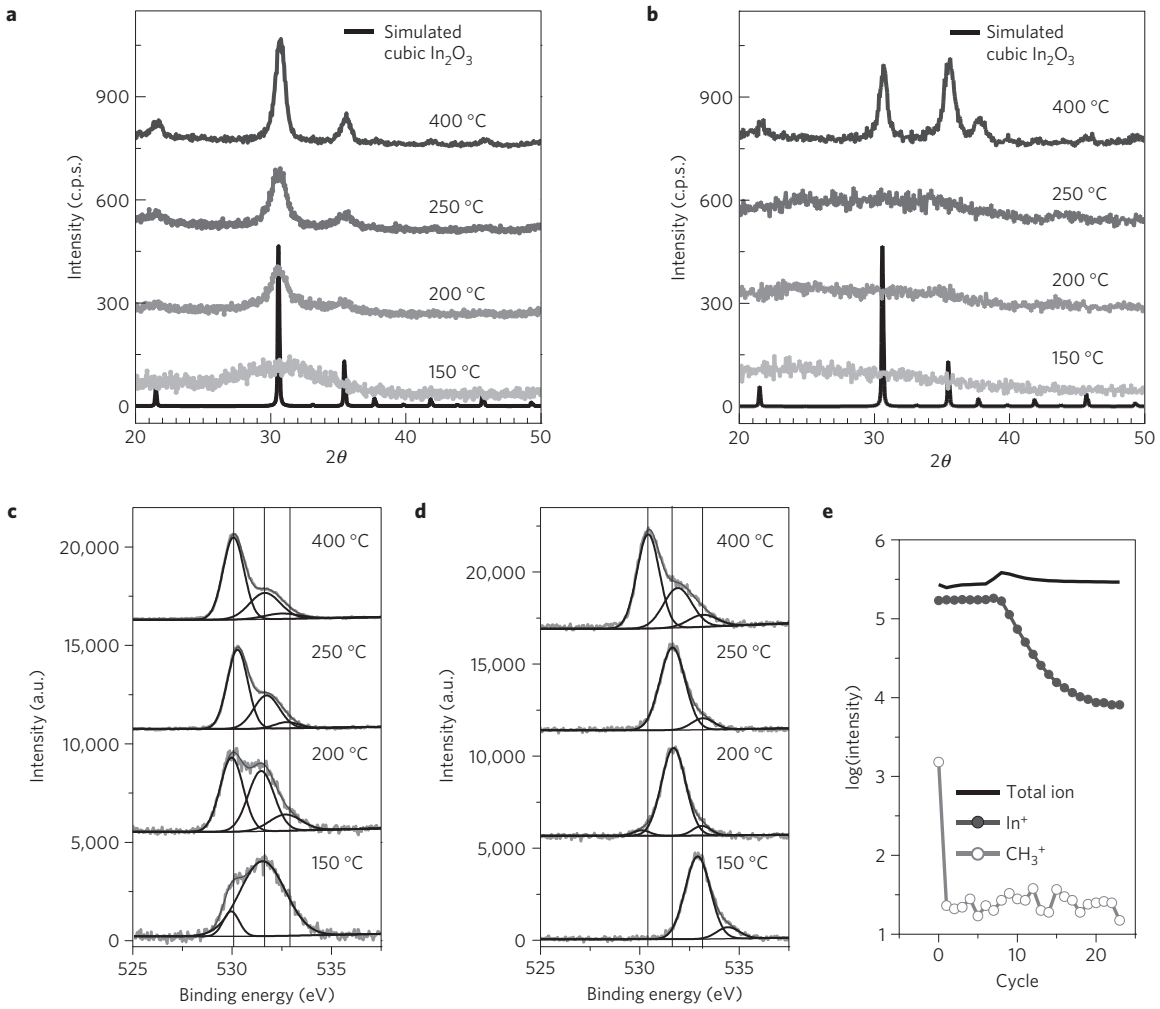

Figure 3 | Surface analysis of In_2O_3 films deposited with both types of precursors. a, GIAXRD results for an In_2O_3 film deposited using a combustion precursor. The bottom black plot is a simulation of the cubic In_2O_3 spectrum. **b**, GIAXRD results for an In_2O_3 film deposited with a conventional precursor. The bottom black plot is a simulation of the cubic In_2O_3 spectrum. **c**,**d**, X-ray photoelectron spectroscopy (XPS) of an In_2O_3 film deposited with a combustion precursor (**c**) and a conventional precursor (**d**) (530.1 eV: M–O–M lattice oxygen, 531.1 eV: M–OH metal hydroxide oxygen, and 532.3 eV: adsorbed oxygen species). **e**, Secondary ion mass spectrometry (SIMS) of an In_2O_3 film deposited with a combustion precursor.

the aforementioned oxide semiconductors, crystalline ITO can be formed at temperatures as low as 200 °C, judging from the GIAXRD and thermal analysis data in Fig. 2a and Supplementary Fig. S2a. As the ITO precursor system is highly oxidizing and used under air, mild post-annealing in a reducing environment is required to obtain high ITO carrier concentrations. By maintaining the combustion-derived ITO films under an H_2 atmosphere at the same temperature as for $T_{anneal} < 300$ °C, or at 300 °C for $T_{anneal} > 300$ °C, significant carrier densities are achieved. The resulting conductivity is plotted versus T_{anneal} in Fig. 2c. For low annealing temperatures ~200 °C, the film conductivity obtained is 0.35 S cm^{-1}. Considering the XRD evidence for complete conversion to crystalline ITO at 200 °C (Supplementary Fig. S2a), the modest conductivity can be attributed to insufficient free-carrier concentrations at these low temperatures. However, a conductivity of 130 S cm^{-1} is obtained at 250 °C, comparable to that of the conducting corrosive polymer PEDOT:PSS, and thermally compatible with commercial high-temperature polymer substrates such as polyether ether ketones, polyimides, and polyarylates[31]. In addition, a continuous increase in conductivity with T_{anneal} is observed for this solution-processed ITO, up to 680 S cm^{-1} for $T_{anneal} = 500$ °C. Although these values are insufficient for transparent data bus lines requiring metal-like conductivity, they suffice for TFT contact electrodes. Solution-processed electrodes based on Au or Ag typically show poor contact resistance for oxide semiconductors versus Al or ITO[47]. As ITO is an excellent contact material for n-type oxide semiconductors, obtaining such contacts via low-temperature solution processing is advantageous.

Optimizing the semiconductor–dielectric interface is crucial for maximum TFT performance by significantly reducing trap states[18,23–25,27,35,48]. Amorphous alumina, known to be solution-processable at low enough temperatures to be compatible with flexible substrates[16], was used here as the TFT gate dielectric and incorporated in devices fabricated with semiconducting In_2O_3 films grown at the lowest combustion temperatures. As shown in Supplementary Fig. S6, a-alumina films deposited at 250 °C and 200 °C exhibit far higher capacitances, 188 nF cm^{-2} and 173 nF cm^{-2}, respectively (measured at 10 kHz), than the 11 nF cm^{-2} of 300 nm SiO_2, along with low leakage currents (~10^{-7} A cm^{-2} at 1 MV cm^{-1}) at low operating voltages (~2 V) and minimal frequency sensitivity of the capacitance (~10% difference from 1 kHz to 1 MHz). A significant TFT mobility enhancement is also observed on changing the dielectric from SiO_2 to a-alumina (Fig. 4b, Supplementary Table S1). Thus, for $T_{anneal} = 250$ °C, μ^{sat} increases from 3.4 to 39.5 cm^2 V^{-1} s^{-1}. The significant reduction in interfacial trap density (D_{it}) from 2.1×10^{12} to 5.9×10^{11} cm^{-2} eV^{-1}, calculated from the subthreshhold swing (S) data, indicates that the principal origin of the increased

Table 1 | Thin-film transistor data for combustion synthesis-derived oxide films and conventional precursor-derived oxide films in p+ Si/300 nm SiO_2/semiconductor devices using 30 nm Al source/drain electrodes.

Conventional precursor				Combustion synthesis-based precursor			
Metal oxide	T_a (°C)	Mobility ($cm^2\ V^{-1}\ s^{-1}$)	I_{on}/I_{off}	Metal oxide	T_a (°C)	Mobility ($cm^2\ V^{-1}\ s^{-1}$)	I_{on}/I_{off}
In_2O_3	400*	0.7*	10^6*	In_2O_3	180	Inactive ($\mu \sim 10^{-6}$)‡	
	200	Inactive			200	0.81	10^6
	250	Inactive ($\mu \sim 10^{-4}$)‡			225	1.81	10^6
	300	2.30	10^4		250	3.37	10^7
	400	5.92	10^2–10^4		300	6.5	10^4
					325	9.4	10^3
$ZnSnO_3$	200	Inactive		$Zn_{0.3}Sn_{0.7}O_{1.7}$	200	Inactive ($\mu \sim 10^{-4}$)‡	
	250	Inactive ($\mu \sim 10^{-5}$)‡			225	0.29	10^4
	300	Inactive ($\mu \sim 10^{-5}$)‡			250	1.76	10^7
	350	0.03	10^4		300	3.03	10^6
	400	1.67	10^7		350	7.02	10^4
					400	7.34	10^3
$InZnO_{2.5}$	250	Inactive ($\mu \sim 10^{-4}$)‡		$In_{0.7}Zn_{0.3}O_{1.35}$	200	Inactive ($\mu \sim 10^{-3}$)‡	
	300	0.22	10^5		225	0.32	10^6
	350	1.37	10^5		250	0.91	10^6
	400	2.14	10^5		300	3.20	10^5
					400	9.78	10^4

Conventional precursor			Combustion synthesis-based precursor		
Metal oxide	T_a (°C)	Conductivity ($S\ cm^{-1}$)	Metal oxide	T_a (°C)	Conductivity ($S\ cm^{-1}$)
$In_{0.9}Sn_{0.1}O_{1.55}$† (ITO)	—	—	$In_{0.9}Sn_{0.1}O_{1.55}$ (ITO)	200	0.35
	—	—		225	15
	—	—		250	130
	300	~100		300	140
	400	~250		400	440
	500	~1,200		500	680

p+ Si/300 nm SiO_2/ITO structures used for four-probe conductivity measurements. *From ref. 27 with 50 nm Au electrode. †From ref. 17. ‡Several devices are inactive and some devices are active with maximum mobilities in parenthesis.

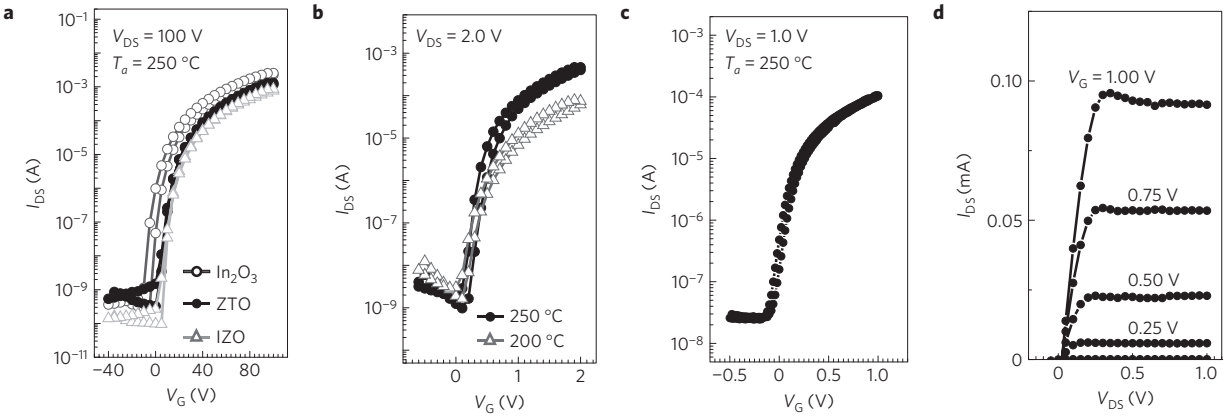

Figure 4 | Transfer and output characteristics of combustion precursor-derived TFTs fabricated with the indicated semiconductors and 2,000 μm channel width, 100 μm channel length Al electrodes. a, Transfer characteristics of In_2O_3, ZTO and IZO devices annealed at 250 °C on 300 nm SiO_2/p+Si substrates. **b**, Transfer characteristics of an In_2O_3 TFT on n++ Si/a-alumina dielectric annealed at the indicated temperatures (38 nm a-alumina for 250 °C, 41 nm a-alumina for 200 °C). **c**,**d**, Transfer characteristics (**c**) and output characteristics (**d**) of an In_2O_3 TFT on 38 nm a-alumina/250 nm ITO/1737F glass annealed at 250 °C.

performance is the improved semiconductor–dielectric interface.

With the present successful integration of low-temperature solution-processed a-alumina as the gate dielectric, it is now possible to demonstrate solution processing of all-oxide TFTs at temperatures below 250 °C, combining a solution-processed oxide gate electrode, dielectric, and semiconductor on Corning 1737F glass substrates. For completion of this top-contact/bottom-gate structure, 30 nm Al source and drain electrodes of 2,000 μm × 100 μm channel dimensions were defined by thermal evaporation. The resulting TFT performance is comparable to that of devices fabricated on highly conducting n++Si gate electrodes with $\mu = 36.2\ cm^2\ V^{-1}\ s^{-1}$ and $I_{on}/I_{off} \sim 10^4$ (Fig. 4c,d). As shown in Supplementary Fig. S3c, this device shows high optical transparency in the visible region ($T > 80\%$).

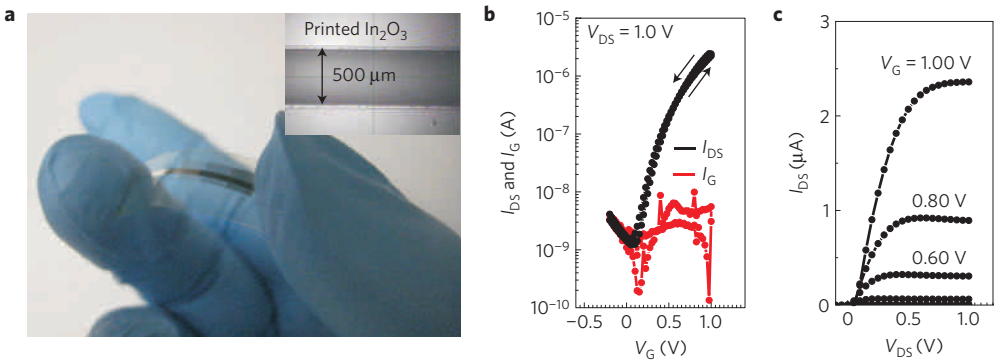

Figure 5 | Flexible combustion-processed In_2O_3 TFTs fabricated on the indicated substrates. a, Optical image of a flexible combustion-processed In_2O_3 device on AryLite (30 nm Al gate electrode/41 nm a-alumina dielectric, with 30 nm Al source and drain electrodes) and optical image of an inkjet printed In_2O_3 line on n++Si/41 nm a-alumina (inset). **b**,**c**, Transfer characteristics (**b**) and output characteristics (**c**) of flexible In_2O_3 TFTs on AryLite/30 nm Al/41 nm a-alumina dielectric.

As noted above, the ultimate goal of solution processing is to realize high-throughput oxide devices on flexible substrates[1,17]. To demonstrate the efficacy of the present approach for flexible circuitry, the In_2O_3 combustion precursor solution was spin-coated on a a-alumina dielectric/30 nm Al/transparent AryLite polyester substrate, followed by annealing at 200 °C (Fig. 5a). The vacuum-deposited 1,000-μm wide 30-nm thick Al gate and a-alumina dielectric were deposited in sequence on the AryLite substrate. The resulting In_2O_3 device performance on the flexible AryLite substrate affords reasonable performance with $\mu^{sat} = 6.0\,cm^2\,V^{-1}\,s^{-1}$ and $I_{on}/I_{off} \sim 10^3$ (Fig. 5b,c). Furthermore, in a preliminary study we validated inkjet printing of the In_2O_3 combustion precursor on n++Si/a-alumina dielectric (Fig. 5a inset). These demonstrations of low-temperature processed In_2O_3 on flexible substrates are doubtless extendable to other substrates and metal oxides.

In conclusion, we have successfully integrated combustion processing with solution deposition of oxide-based macroelectronics. The unique self-generating energy characteristics of this process enable a significant reduction of processing temperatures versus conventional thermal condensation syntheses. For example, semiconducting In_2O_3 can be annealed at temperatures as low as 200 °C to yield TFTs with mobilities approaching $1\,cm^2\,V^{-1}\,s^{-1}$ on a 300-nm SiO_2 gate dielectric. Combining this 200 °C processed In_2O_3 semiconductor with an optimized, low-temperature processed gate dielectric with significantly higher capacitance affords In_2O_3 TFTs with a mobility of $\sim$13 $cm^2\,V^{-1}\,s^{-1}$ at operating voltages as low as $\sim$2 V. Furthermore, this work establishes significant generality for the low-temperature combustion synthesis of other oxide semiconductors and conductors useful in the fabrication of flexible, transparent circuitry.

Methods

Precursor synthesis and characterization. All reagents were purchased from Aldrich and used as received. For acetylacetone-based fuel systems, the In, Zn and Sn precursors were prepared, respectively, by dissolving 352.2 mg $In(NO_3)_3 \cdot 2.85\ H_2O$, 297.5 mg $Zn(NO_3)_2 \cdot 6H_2O$ or 189.6 mg $SnCl_2$ with 80.1 mg NH_4NO_3 in 5 ml 2-methoxyethanol, then adding 0.20 ml acetylacetone. The pure tin(II/IV) nitrates are reported to be unstable under an ambient environment[49,50]. After completely dissolving the metal salt, 114 μl (for In and Zn) or 57 μl (for Sn) of 14.5 M NH_3(aq) was added and the solution was aged for 12 h. In the case of the urea-based Zn and Sn precursors, 297.5 mg $Zn(NO_3)_2 \cdot 6H_2O$ and 100.1 mg urea, for Zn, or 189.6 mg $SnCl_2$, 60.1 mg urea and 80.1 mg NH_4NO_3, for Sn, respectively, were dissolved in 5 ml 2-methoxyethanol and aged for 72 h. For the IZO, ZTO, and ITO precursors, the In:Zn = 7:3, In:Sn = 9:1 and Zn:Sn = 7:3 ratio was achieved by mixing the two component solutions and stirring 1h before film casting.

Thermal analyses were carried out on 10–15 mg samples prepared from evaporated precursor solutions. The heating rate was 10 °C min^{-1} under a 20 ml min^{-1} air flow using an aluminium sample container. The TGA and DTA measurements were performed on a Shimadzu TGA-50 thermogravimetric analyser and a Shimadzu DTA-50 thermal analyser, respectively. Using the standard instrumental configuration, the TGA thermocouple is located 5 mm below the sample holder.

Film fabrication and characterization. The In_2O_3, IZO, and ZTO precursor solutions, with total metal concentrations of 0.05 M, were spin-coated on n++ Si wafers (Montco Silicon Technologies) at 3,500 r.p.m. for 35 s and then annealed at the desired temperature (T_{anneal} = 150–400 °C) for 30 min under air. Amorphous alumina dielectric films were grown using a procedure similar to that reported in the literature ($Al(NO)_3 \cdot 9H_2O$ in 2-methoxyethanol; ref. 16). The a-alumina films were spin-coated using a 0.1 M $Al(NO_3)_3 \cdot 9H_2O$ precursor solution on n++-Si or ITO/1737F glass and annealed at 200 or 250 °C for 30 min for each layer, with 1 min initial oxygen plasma treatment. The ITO film was fabricated by spin-coating the precursor solution with a total metal concentration of 0.4 M solution at 2,000 r.p.m. for 35 s, and then annealing at the desired temperature (T_{anneal} = 200–500 °C) for 30 min under air. These processes were repeated as necessary to achieve the desired film thickness. For final annealing, the ITO films were annealed for 1 h under H_2 at the same temperature as the air annealing for $T_{anneal} < 300$ °C or at 300 °C for $T_{anneal} > 300$ °C.

Film surface morphologies were imaged with a Veeco Dimension ICON PT AFM System and a Hitachi S-4800-II FE-SEM. GIAXRD scans were measured with a Rigaku ATX-G Thin-Film Diffraction Workstation using Cu Kα radiation coupled to a multilayer mirror. Film thicknesses were determined by profilometry for ITO and by X-ray reflectivity or ellipsometry for thin dielectric and semiconductor films. Optical spectra were acquired with a Cary 5000 ultraviolet–visible–near-infrared spectrophotometer. XPS spectra were recorded on an Omicron ESCA Probe system with a base pressure of 8×10^{-10} mbar (UHV), using a monochromated Al Kα X-ray source at $h\nu$ = 1,486 eV. Quantitative secondary ion mass spectroscopic (SIMS) analysis was performed on a MATS quadrupole SIMS instrument using a 15 keV Ga^+ ion source.

TFT fabrication and electrical measurements. Conductivities of the ITO thin films on 300 nm SiO_2/Si were measured with a Keithley 2182A nanovoltmeter and 6221 current source using the four-probe method. The leakage current and capacitance of a-alumina were measured with a Keithley 6430 subfemtometer and an HP4192A LF using thermally evaporated 50 nm thick Au electrodes (200 μm × 200 μm). Semiconducting oxide thin films were deposited on various substrates, as described in Supplementary Table S1. For printing of In_2O_3 semiconductor channels, 500 μm × 5 mm lines were printed with a Fujifilm Dimatix Materials Printer DMP-2800. The final 30 nm Al source and drain electrode were thermally evaporated for 2,000 μm × 100 μm (common gate with n++Si, p+Si or ITO) or 1,000 μm × 100 μm channels (1,000 μm patterned 30 nm Al gate). TFT device characterization was performed on a custom probe station in air with a Keithley 6430 subfemtometer and a Keithley 2400 source meter, operated by a locally written Labview program and GPIB communication.

TFT performance parameters, saturation mobility (μ_{Sat}), subthreshhold swing (S) and interfacial trap density (D_{it}), were evaluated with the conventional metal–oxide–semiconductor field effect transistor (MOSFET) model described in equations (2) and (3) (ref. 51).

$$\mu_{Sat} = \left(\frac{\partial\sqrt{I_{DS}}}{\partial V_G}\right)^2 \frac{2L}{WC_i} \quad (2)$$

$$S = \frac{dV_G}{d(\log I_{SD})} \approx \ln 10 \frac{kT}{q}\left[1 + \frac{qD_{it}}{C_i}\right] \quad (3)$$

Received 9 November 2010; accepted 17 March 2011; published online 17 April 2011

References

1. Mitzi, D. B. *Solution Processing of Inorganic Materials* (Wiley, 2009).
2. Reuss, R. H. *et al.* Macroelectronics: Perspectives on technology and applications. *Proc. IEEE* **93,** 1239–1256 (2005).
3. Sun, Y. G. & Rogers, J. A. Inorganic semiconductors for flexible electronics. *Adv. Mater.* **19,** 1897–1916 (2007).
4. Bae, S. *et al.* Roll-to-roll production of 30-inch graphene films for transparent electrodes. *Nature Nanotech.* **5,** 574–578 (2010).
5. Ortiz, R. P., Facchetti, A. & Marks, T. J. High-*k* organic, inorganic, and hybrid dielectrics for low-voltage organic field-effect transistors. *Chem. Rev.* **110,** 205–239 (2010).
6. Mannsfeld, S. C. B. *et al.* Highly sensitive flexible pressure sensors with microstructured rubber dielectric layers. *Nature Mater.* **9,** 859–864 (2010).
7. Arias, A. C., MacKenzie, J. D., McCulloch, I., Rivnay, J. & Salleo, A. Materials and applications for large area electronics: Solution-based approaches. *Chem. Rev.* **110,** 3–24 (2010).
8. Yan, H. *et al.* A high-mobility electron-transporting polymer for printed transistors. *Nature* **457,** 679–686 (2009).
9. Naber, R. C. G. *et al.* High-performance solution-processed polymer ferroelectric field-effect transistors. *Nature Mater.* **4,** 243–248 (2005).
10. Faber, H. *et al.* Low-temperature solution-processed memory transistors based on zinc oxide nanoparticles. *Adv. Mater.* **21,** 3099–3104 (2009).
11. Rivnay, J. *et al.* Large modulation of carrier transport by grain-boundary molecular packing and microstructure in organic thin films. *Nature Mater.* **8,** 952–958 (2009).
12. Sakanoue, T. & Sirringhaus, H. Band-like temperature dependence of mobility in a solution-processed organic semiconductor. *Nature Mater.* **9,** 736–740 (2010).
13. Shimoda, T. *et al.* Solution-processed silicon films and transistors. *Nature* **440,** 783–786 (2006).
14. van der Wilt, P. *et al.* Low-temperature polycrystalline silicon thin-film transistors and circuits on flexible substrates. *MRS Bull.* **31,** 461–465 (2006).
15. Ju, S. Y. *et al.* Fabrication of fully transparent nanowire transistors for transparent and flexible electronics. *Nature Nanotech.* **2,** 378–384 (2007).
16. Pal, B. N., Dhar, B. M., See, K. C. & Katz, H. E. Solution-deposited sodium beta-alumina gate dielectrics for low-voltage and transparent field-effect transistors. *Nature Mater.* **8,** 898–903 (2009).
17. Cho, J. H. *et al.* Printable ion-gel gate dielectrics for low-voltage polymer thin-film transistors on plastic. *Nature Mater.* **7,** 900–906 (2008).
18. Bong, H. *et al.* High-mobility low-temperature ZnO transistors with low-voltage operation. *Appl. Phys. Lett.* **96,** 192115 (2010).
19. Alam, M. J. & Cameron, D. C. Investigation of annealing effects on sol–gel deposited indium tin oxide thin films in different atmospheres. *Thin Solid Films* **420,** 76–82 (2002).
20. Wu, Y. L., Li, Y. N. & Ong, B. S. A simple and efficient approach to a printable silver conductor for printed electronics. *J. Am. Chem. Soc.* **129,** 1862–1863 (2007).
21. Hu, L., Hecht, D. S. & Grüner, G. Carbon nanotube thin films: Fabrication, properties, and applications. *Chem. Rev.* **110,** 5790–5844 (2010).
22. Nomura, K. *et al.* Room-temperature fabrication of transparent flexible thin-film transistors using amorphous oxide semiconductors. *Nature* **432,** 488–492 (2004).
23. Nomura, K. *et al.* Thin-film transistor fabricated in single-crystalline transparent oxide semiconductor. *Science* **300,** 1269–1272 (2003).
24. Wang, L. *et al.* High-performance transparent inorganic–organic hybrid thin-film n-type transistors. *Nature Mater.* **5,** 893–900 (2006).
25. Lee, C. G. & Dodabalapur, A. Solution-processed zinc–tin oxide thin-film transistors with low interfacial trap density and improved performance. *Appl. Phys. Lett.* **96,** 243501 (2010).
26. Choi, C. G., Seo, S. J. & Bae, B. S. Solution-processed indium-zinc oxide transparent thin-film transistors. *Electrochem. Solid-State Lett.* **11,** H7–H9 (2008).
27. Kim, H. S., Byrne, P. D., Facchetti, A. & Marks, T. J. High performance solution-processed indium oxide thin-film transistors. *J. Am. Chem. Soc.* **130,** 12580–12581 (2008).
28. Lee, D. H., Chang, Y. J., Herman, G. S. & Chang, C. H. A general route to printable high-mobility transparent amorphous oxide semiconductors. *Adv. Mater.* **19,** 843–847 (2007).
29. Ong, B. S., Li, C. S., Li, Y. N., Wu, Y. L. & Loutfy, R. Stable, solution-processed, high-mobility ZnO thin-film transistors. *J. Am. Chem. Soc.* **129,** 2750–2751 (2007).
30. Seo, S. J., Choi, C. G., Hwang, Y. H. & Bae, B. S. High performance solution-processed amorphous zinc tin oxide thin film transistor. *J. Phys. D* **42,** 035106 (2009).
31. MacDonald, W. A. Engineered films for display technologies. *J. Mater. Chem.* **14,** 4–10 (2004).
32. Jeong, S., Ha, Y. G., Moon, J., Facchetti, A. & Marks, T. J. Role of gallium doping in dramatically lowering amorphous-oxide processing temperatures for solution-derived indium zinc oxide thin-film transistors. *Adv. Mater.* **22,** 1346–1350 (2010).
33. Kim, H. S. *et al.* Low-temperature solution-processed amorphous indium tin oxide field-effect transistors. *J. Am. Chem. Soc.* **131,** 10826–10827 (2009).
34. Aksu, Y. & Driess, M. A low-temperature molecular approach to highly conductive tin-rich indium tin oxide thin films with durable electro-optical performance. *Angew. Chem. Int. Ed.* **48,** 7778–7782 (2009).
35. Meyers, S. T. *et al.* Aqueous inorganic inks for low-temperature fabrication of ZnO TFTs. *J. Am. Chem. Soc.* **130,** 17603–17609 (2008).
36. Hoffmann, R. C., Differ, S., Issanin, A. & Schneider, J. J. Solution processed ZnO—challenges in processing and performance on flexible substrates. *Phys. Status Solidi A* **207,** 1590–1595 (2010).
37. Asakuma, N., Fukui, T., Toki, M. & Imai, H. Low-temperature synthesis of ITO thin films using an ultraviolet laser for conductive coating on organic polymer substrates. *J. Sol–Gel Sci. Technol.* **27,** 91–95 (2003).
38. Merzhanov, A. G. The chemistry of self-propagating high-temperature synthesis. *J. Mater. Chem.* **14,** 1779–1786 (2004).
39. Tukhtaev, R. K. *et al.* Metal sulfide synthesis by self-propagating combustion of sulphur-containing complexes. *Inorg. Mater.* **38,** 985–991 (2002).
40. Yi, H. C. & Moore, J. J. Self-propagating high-temperature (combustion) synthesis (SHS) of powder-compacted materials. *J. Mater. Sci.* **25,** 1159–1168 (1990).
41. Epifani, M., Melissano, E., Pace, G. & Schioppa, M. Precursors for the combustion synthesis of metal oxides from the sol–gel processing of metal complexes. *J. Eur. Ceram. Soc.* **27,** 115–123 (2007).
42. Sato, T. Preparation and thermal decomposition of indium hydroxide. *J. Therm. Anal. Calorim.* **82,** 775–782 (2005).
43. Pramanik, N. C., Das, S. & Kumar Biswas, P. The effect of Sn(IV) on transformation of co-precipitated hydrated In(III) and Sn(IV) hydroxides to indium tin oxide (ITO) powder. *Mater. Lett.* **56,** 671–679 (2002).
44. Donley, C. *et al.* Characterization of indium–tin oxide interfaces using X-ray photoelectron spectroscopy and redox processes of a chemisorbed probe molecule: Effect of surface pretreatment conditions. *Langmuir* **18,** 450–457 (2002).
45. Kamiya, T., Nomura, K. & Hosono, H. Origins of high mobility and low operation voltage of amorphous oxide TFTs: Electronic structure, electron transport, defects and doping. *J. Display Technol.* **5,** 273–288 (2009).
46. Hosono, H., Nomura, K., Ogo, Y., Uruga, T. & Kamiya, T. Factors controlling electron transport properties in transparent amorphous oxide semiconductors. *J. Non-Cryst. Solids* **354,** 2796–2800 (2008).
47. Ip, K. *et al.* Contacts to ZnO. *J. Cryst. Growth* **287,** 149–156 (2006).
48. Cui, Y., Zhong, Z. H., Wang, D. L., Wang, W. U. & Lieber, C. M. High performance silicon nanowire field effect transistors. *Nano Lett.* **3,** 149–152 (2003).
49. Addison, C. C. & Simpson, W. B. Tin(IV) nitrate: the relation between structure and reactivity of metal nitrates. *J. Chem. Soc.* 598–602 (1965).
50. Donaldson, J.D. & Moser, W. Basic tin(II) nitrate. *J. Chem. Soc.* 1996–2000 (1961).
51. Greve, D. W. *Field Effect Devices and Application: Devices for Portable, Low-Power, and Imaging Systems* (Prentice-Hall, 1988).

Acknowledgements

The research was supported by the MRSEC program of NSF (DMR-0520513) at the Northwestern University Materials Research Center and by AFOSR (FA9550-08-1-0331). Microscopy and XPS studies were performed in the EPIC, NIFTI, KECK-II facilities of NUANCE Center at Northwestern University. NUANCE Center is supported by NSF-NSEC, NSF-MRSEC, Keck Foundation, the State of Illinois, and Northwestern University.

Author contributions

M-G. Kim, M. G. Kanatzidis, A.F. and T.J.M. designed the research. M-G. Kim carried out the experiments. M-G. Kim, M. G. Kanatzidis, A.F. and T.J.M. analysed the data and co-wrote the manuscript.

Additional information

The authors declare no competing financial interests. Supplementary information accompanies this paper on www.nature.com/naturematerials. Reprints and permissions information is available online at http://npg.nature.com/reprintsandpermissions. Correspondence and requests for materials should be addressed to M. G. Kanatzidis, A.F. or T.J.M.